An accuracy assessment of different rigid body image registration methods and robotic couch positional corrections using a novel phantom

Sankar Arumugam[a)]
Liverpool and Macarthur Cancer Therapy Centres and Ingham Institute, New South Wales 2170, Australia

Michael G. Jameson
Liverpool and Macarthur Cancer Therapy Centres and Ingham Institute, New South Wales 2170, Australia and Centre for Medical Radiation Physics, University of Wollongong, Wollongong, New South Wales 2522, Australia

Aitang Xing
Liverpool and Macarthur Cancer Therapy Centres and Ingham Institute, New South Wales 2170, Australia

Lois Holloway
Liverpool and Macarthur Cancer Therapy Centres and Ingham Institute, New South Wales 2170, Australia; Centre for Medical Radiation Physics, University of Wollongong, Wollongong, New South Wales 2522, Australia; University of New South Wales, Sydney, New South Wales 2052, Australia; and Institute of Medical Physics, School of Physics, University of Sydney, Sydney, New South Wales 2006, Australia

(Received 20 August 2012; revised 2 November 2012; accepted for publication 12 January 2013; published 8 February 2013)

Purpose: Image guided radiotherapy (IGRT) using cone beam computed tomography (CBCT) images greatly reduces interfractional patient positional uncertainties. An understanding of uncertainties in the IGRT process itself is essential to ensure appropriate use of this technology. The purpose of this study was to develop a phantom capable of assessing the accuracy of IGRT hardware and software including a 6 degrees of freedom patient positioning system and to investigate the accuracy of the Elekta XVI system in combination with the HexaPOD robotic treatment couch top.
Methods: The constructed phantom enabled verification of the three automatic rigid body registrations (gray value, bone, seed) available in the Elekta XVI software and includes an adjustable mount that introduces known rotational offsets to the phantom from its reference position. Repeated positioning of the phantom was undertaken to assess phantom rotational accuracy. Using this phantom the accuracy of the XVI registration algorithms was assessed considering CBCT hardware factors and image resolution together with the residual error in the overall image guidance process when positional corrections were performed through the HexaPOD couch system.
Results: The phantom positioning was found to be within 0.04 ($\sigma = 0.12$)°, 0.02 ($\sigma = 0.13$)°, and −0.03 ($\sigma = 0.06$)° in X, Y, and Z directions, respectively, enabling assessment of IGRT with a 6 degrees of freedom patient positioning system. The gray value registration algorithm showed the least error in calculated offsets with maximum mean difference of $-0.2(\sigma = 0.4)$ mm in translational and $-0.1(\sigma = 0.1)$° in rotational directions for all image resolutions. Bone and seed registration were found to be sensitive to CBCT image resolution. Seed registration was found to be most sensitive demonstrating a maximum mean error of $-0.3(\sigma = 0.9)$ mm and $-1.4(\sigma = 1.7)$° in translational and rotational directions over low resolution images, and this is reduced to $-0.1(\sigma = 0.2)$ mm and $-0.1(\sigma = 0.79)$° using high resolution images.
Conclusions: The phantom, capable of rotating independently about three orthogonal axes was successfully used to assess the accuracy of an IGRT system considering 6 degrees of freedom. The overall residual error in the image guidance process of XVI in combination with the HexaPOD couch was demonstrated to be less than 0.3 mm and 0.3° in translational and rotational directions when using the gray value registration with high resolution CBCT images. However, the residual error, especially in rotational directions, may increase when the seed registration is used with low resolution images.
 [http://dx.doi.org/10.1118/1.4789490]

Key words: cone-beam CT, image guidance, phantoms, image registration, image resolution

I. INTRODUCTION

Image guided radiotherapy (IGRT) is the name given to the imaging and guidance procedures employed before, during and after radiotherapy treatment.[1] There are a number of different technologies used for IGRT. Cone beam computed tomography (CBCT) using a megavoltage treatment beam (MVCBCT) or an orthogonal kilovoltage beam (kVCBCT), as well as planar MV and kV images are commonly used in most radiotherapy centers. Less common technologies include MRI,[2] robotic ultrasound guidance,[1,3,4] CT on rails,[4] Tomotherapy,[5] and optical imaging.[6] Modern linear accelerators (linacs) come equipped with kVCBCT known as onboard imager (OBI) and x-ray volume imaging (XVI) on the Varian

(Varian Medical systems, Palo Alto) and Elekta (Elekta Pty Limited, Crawly, UK) systems, respectively.[7]

Image acquisition, reconstruction, and registration are three components in modern IGRT systems. In general, the patient positional offsets derived from an image guidance system are corrected through a linac patient support system (PSS). Typical PSSs provide four spatial degrees of freedom; translation in each direction, and rotation about the Z axis.[8] This is sufficient to correct for translational offsets with which modern fixation have been demonstrated to be less than 2.1 ± 2.7, 2.4 ± 5.6, 1.4 ± 2.0 mm for pelvic, thoracic, and head and neck malignancies, respectively.[9–11] Rotational offsets have been reported for the same tumor sites with systematic and random errors ranging from 0.4° to 1.1° and 1.0° to 2.2°.[12] A robotic PSS with six degrees of freedom (6DOF) was first proposed in 1998.[13] All of the major radiotherapy treatment vendors now supply PSSs that provide 6DOF motion (x, y, z, pitch, roll, and yaw). The use of robotic 6DOF PSSs with three-dimensional (3D) imaging has been shown to improve patient positioning from 4.1 ± 2.4 to 0.9 ± 0.5 mm when using appropriate immobilization.[14]

In IGRT, the robotic PSS movements are guided by the positional offsets derived from the image registration process.[15] Commercial image guidance systems come with various automatic rigid body image registration algorithms to calculate the positional offsets between reference and verification image sets. The Elekta XVI system comes with three automatic image registration methods; gray value, bone, and seeds.[2,16] Depending on the clinical requirement different registration methods can be selected to align image sets.

IGRT allows reduction of treatment margins. However, this reduction means that any error in patient positioning becomes more significant.[17,18] It is therefore important that IGRT and patient positioning systems are rigorously tested at the implementation stage and routinely thereafter.[8] There are a number of products available for testing laser/image/treatment isocenter coincidence or phantom localization and repositioning with PSS shifts.[8] These products include the MIMI (Standard Imaging, Middleton, WI), PentaGuide (Modus Medical Devices, Inc., London, Canada), and IsoCube (CIRS, Norfolk, VA). These phantoms are placed on the PSS and imaged in a known offset position with respect to a reference image. The image is registered to the reference image, and based on the registration results, a correction is applied using the PSS. The IGRT system is determined to be functioning correctly if the phantom position then matches the reference image position with respect to lasers. These phantoms work well for a standard PSS with 4DOF. However, if the PSS has 6DOF, then it is difficult to accurately and precisely position the phantom in a known offset position that will test the accuracy of the angular corrections.

In this work, we present the design and development of a phantom to undertake this initial assessment and future quality assurance as well as an assessment of the accuracy and reproducibility of the automatic registration techniques and couch corrections provided by the Elekta Synergy XVI and HexaPOD systems.

II. MATERIALS AND METHODS

II.A. Image guidance system

An Elekta-Synergy linac (Elekta Limited, Crawley, UK) equipped with kV imaging and capable of acquiring planar, motion, and volume images was used in this study. CBCT imaging and registration between the reference and verification images with the Elekta XVI v4.5 software was investigated. The XVI software enables the various imaging parameters and reconstruction resolutions to be selected by the user. CBCT images can be reconstructed at high (0.5 mm), medium (1 mm), and low (2 mm) resolutions. Three rigid body registration algorithms (namely, gray value, bone, and seed matching) are available for matching the reference and verification image datasets. The gray value automatic registration technique uses a gray level correlation ratio algorithm.[19] The bone registration technique uses a chamfer matching algorithm.[20] The seeds matching algorithm uses the same chamfer matching algorithm as the bone algorithm, except the algorithm has been optimized to match small objects of high density that are nonlinearly separated. Further details about the functional details of the XVI system and the implementation of various image registration algorithms can be found in Refs. 21 and 22.

II.B. Robotic couch system

A HexaPOD robotic couch top (Elekta-Medical intelligence, GmbH, Germany) with 6DOF was considered in this study. The maximum range of translational and rotational movements was 30 mm and 3°, respectively, on either side of the isocenter along all three axes. Further details on the HexaPOD system can be found in Ref. 14.

II.C. Hexacheck phantom

An inhouse constructed phantom (Fig. 1) was developed in this study to enable assessment of the translational and rotational offsets calculated by the XVI software and shifts undertaken by the HexaPOD couch. The phantom consists of two main parts: The main body and rotational mount.

II.C.1. Body of the phantom

The main body of the phantom is detailed in Figs. 1(a) and 1(b). Bone simulating structures consisting of two cylindrical shapes with length of 25 mm and diameters of 7 and 10 mm were inserted. Similarly, three small cylinders simulating Civco prostate seeds all with dimensions 1.2 mm in diameter and 3 mm in length were embedded inside the phantom. The bone and seed simulating structures were fabricated using a commercial dental putty compound, which uses calcium phosphosilicate as an active component and produces CT numbers close to those of bone. Figures 1(a) and 1(b) show the schematic of the phantom and its internal structures. Three reference lead markers, one at the top and two at either

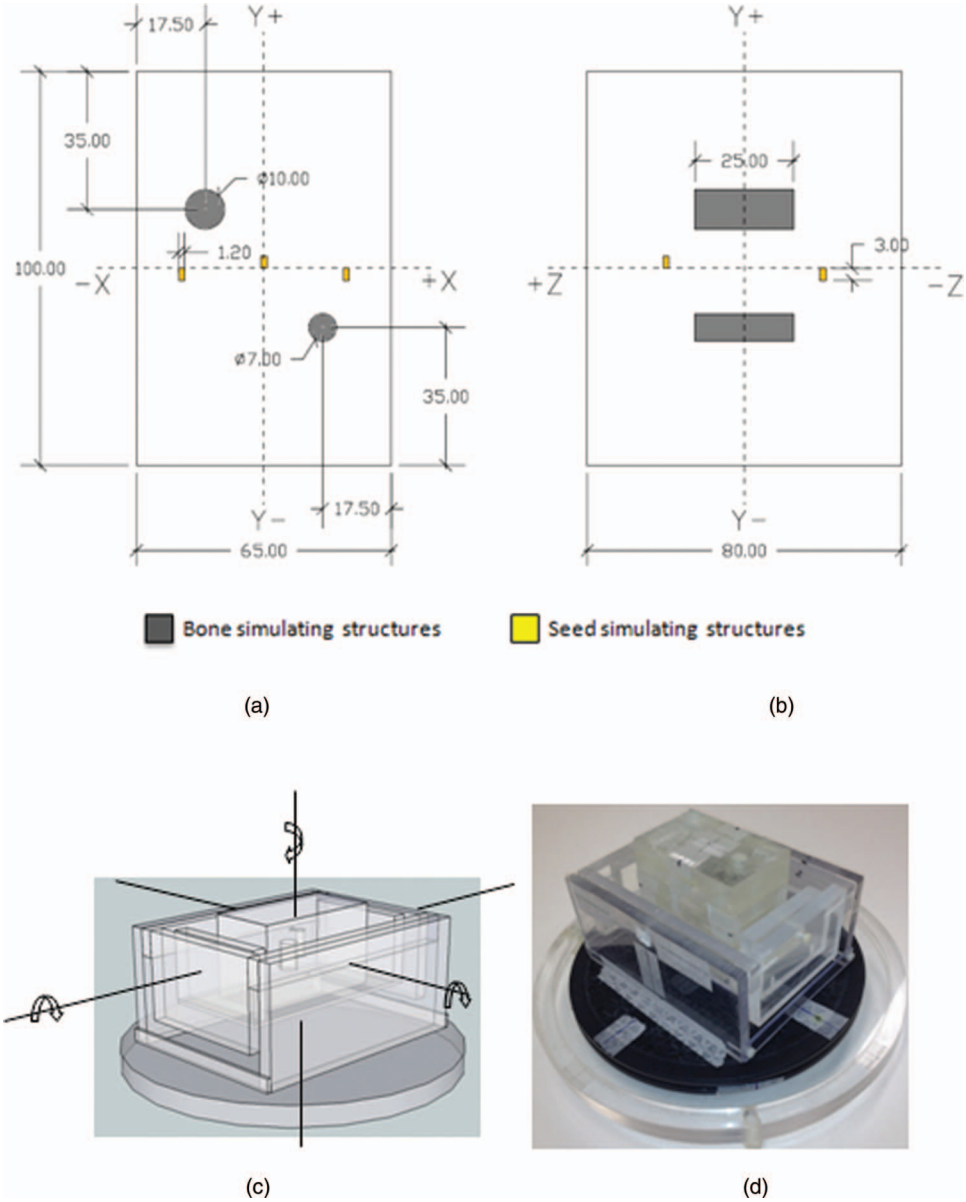

FIG. 1. Schematic diagram of phantom body ((a) top view and (b) side view). (c) Schematic diagram of the phantom mounted on a rotatable platform. (d) Picture of the prototype version of phantom developed inhouse.

side of the phantom, identify the center of the phantom in the CT image dataset.

II.C.2. Rotatable phantom mount

The mount, Fig. 1(c), is capable of rotating independently about the X, Y, and Z axes and the level of the whole mount can be aligned using three leveling screws. The range of rotation about the X and Y axes is limited to ±13° and ±25°, respectively, with a full 360° rotation possible about the Z axis. The intersection of the X, Y, and Z pivot axes of the platform aligns with the center of the phantom such that the phantom rotates about its center on all axes [Fig. 1(d)]. Calibrated reference lines were marked at appropriate locations on the platform to enable the phantom to be easily and accurately rotated to preset angles of up to ±3° for each axes matching the range of rotation available with the HexaPOD couch system. The translational displacement of the phantom was realized through linear movement of the linac couch system.

II.D. Rotational accuracy and reproducibility of the phantom positioning

To verify the accuracy and reproducibility in positioning the phantom to preset angles, three different users were asked to position the phantom to the angles given in Table I. The agreement between the intended and actual angles in X and Y directions was determined using a calibrated digital level placed along the appropriate direction on the top surface of

TABLE I. Preset rotational offsets set by different users to verify the rotational accuracy of the phantom.

	Rotational offsets (deg)		
Number of sets	X	Y	Z
Set1	1.0	− 3.0	1.0
Set2	2.0	1.0	− 2.0
Set3	3.0	− 2.0	2.0
Set4	− 1.0	2.0	− 3.0
Set5	− 2.0	3.0	− 1.0
Set6	− 3.0	1.0	3.0

TABLE II. Key characteristics of various CBCT image acquisition protocols used in the study.

Protocol	X-ray energy (kV)	Bowtie filter	Scan angle (deg)	FOV	mAs
Head and neck	100	No	200	Small	36.6
Fast head and neck	100	No	200	Small	18.3
Pelvis – seeds	120	No	360	Small	117
Pelvis – medium	120	Yes	360	Large	416
Pelvis – large	120	Yes	360	Medium	416
Chest – medium	120	Yes	360	Large	116
Chest – large	120	Yes	360	Large	116

the phantom. The rotational accuracy about the Z axis was tested by measuring the arc length between the reference and marker lines on the rotating base plate [Fig. 1(d)].

II.E. Reference image dataset of the phantom

To provide a reference image dataset, the phantom was leveled and aligned to 0° in all three axes and scanned in a Siemens-Somatom (Siemens AG, Erlangen, Germany) CT scanner. Images were acquired with 1 mm slice thickness in helical mode and reconstructed at 1 mm slice spacing. The images were transferred to the XiO, v4.6 (Elekta CMS software, Inc., MO) treatment planning system and the isocenter was defined at the center of the phantom image with the guidance of the lead markers. The image and isocenter position was exported to the XVI application and used as the reference dataset for this study.

II.F. Uncertainties due to hardware setup and the gray value registration

The phantom was set up on the HexaPOD couch in the reference position. The uncertainty due to software registration and positioning of the detector and source was studied by scanning the phantom with a standard CBCT protocol. A head and neck imaging protocol was used and reconstructed with high resolution to generate the "standard CBCT" dataset. To test the effect of hardware positioning on registration uncertainty, the gray value algorithm was used as is the most accurate of the registration methods. Different components of the imaging and registration processes were then repeated as detailed below:

1. Uncertainty due to both the imaging and registration process was determined by repeating the CBCT imaging and registration of these images with the reference image data five times.
2. Uncertainty due to the positioning of kV source and detector arms was determined by retracting and repositioning the kV source arm on each of five occasions followed by imaging and registration and then repeating for the kV detector arm.
3. Uncertainty due to different image acquisition conditions was determined by acquiring images for each of the image acquisition conditions detailed in Table II followed by registration to the reference image with the XVI software.

II.G. Accuracy of different registration methods and image resolutions

Accuracy of the three registration methods (gray value, bone, and seeds) and image resolution options (low, medium, and high) available in the XVI software was also assessed. The translational and rotational (T&R) errors calculated by the software when gray value, bone, and seed registration methods were used for image registration were studied using image data acquired in Sec. II.F. All combinations of CBCT resolution and registration algorithm were investigated to calculate the associated mean error. For gray value registration, the total body of the phantom was defined as the ROI. This ensured nonmovable parts of the phantom were not considered in the image registration. For bone registration, the region encompassing the bone simulating structures was defined as the ROI. Due to the design of the phantom this region also includes the seed simulating structure in the ROI. For seed registration, the region encompassing only seeds was defined as the ROI. To ensure the same starting point for each registration method previous registration results were "reset" using the option available in the XVI software.

II.H. Accuracy of positional Offsets calculated by XVI

The accuracy of the XVI software in calculating T&R errors was tested by offsetting the phantom from its reference position. The positional offsets of the phantom were simulated in the following three scenarios:

1. 3D translational offsets,
2. 3D rotational offsets,
3. Combined 3D translational and rotational offsets.

The magnitudes and number of offsets simulated under each scenario are shown in Table III. The offsets were designed to encompass reported setup errors for common treatment sites with a maximum translation of 15 mm in an extreme case.[12] Verification images for all these offsets were acquired using a CBCT head and neck protocol.

TABLE III. Translational and rotational offsets used in the study to test the accuracy offsets predicted by XVI software.

		Translational offsets (mm)			Rotational offsets (deg)		
Offset scenario		TX	TY	TZ	RX	RY	RZ
3D translation	Set1	−15	10	5	0	0	0
	Set2	3	−15	−10	0	0	0
	Set3	−5	3	15	0	0	0
	Set4	10	−5	−3	0	0	0
3D rotation	Set5	0	0	0	1	2	−3
	Set6	0	0	0	−2	−3	1
	Set7	0	0	0	−3	1	2
Combined 3D	Set8	−15	10	5	1	2	−3
translation and	Set9	3	−15	−10	−2	−3	1
rotation	Set10	−5	3	15	−3	1	2

II.I. Residual error after corrections using the robotic couch

The overall residual error in the image guided process after positional corrections performed through the HexaPOD couch system was also investigated. The positional errors calculated by XVI for high resolution CBCT images with gray value registration were corrected through the HexaPOD couch system for each of the offsets listed in Table III. To simulate treatment conditions, a load of 150 kg was placed on the couch over a distance of 2 m. To determine the remaining uncertainty after the positional corrections, a repeat CBCT was performed. The acquired verification images were registered with the reference image dataset using gray value registration algorithm and the residual T&R error determined using the XVI software.

III. RESULTS

III.A. Accuracy and reproducibility of phantom rotation

The difference between the set and actual angles of the phantom for different magnitudes of rotation about the X, Y, and Z axes from the three different users is shown in Fig. 2. The difference ranged from −0.2° to 0.3° in the X and Y directions whereas in the Z direction the difference was restricted to between −0.1° and 0.1°. The mean difference and standard deviation (σ) between set and actual angles in X, Y, and Z directions were 0.04°($\sigma = 0.12°$), 0.02°($\sigma = 0.13°$), and −0.03°($\sigma = 0.06°$), respectively. Table IV shows the expanded uncertainty in phantom positioning in X, Y, and Z directions. The uncertainty in phantom positioning was less than 0.06° in any direction.

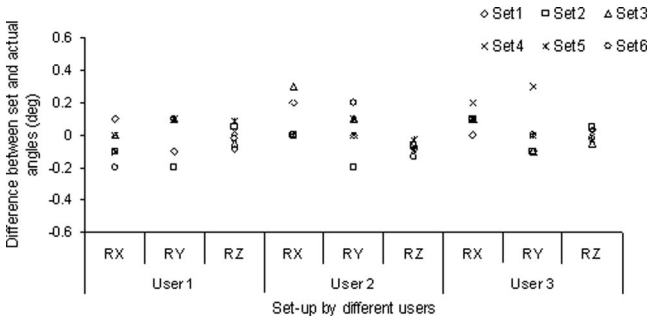

FIG. 2. Difference between the actual and set angles when the phantom was rotated to different angles in x, y and z directions by three different users.

III.B. Uncertainties

Table V shows the positional offset of the phantom, calculated by the XVI software, on the treatment couch with respect to the reference image. Maximum positional difference of 0.2 mm in translational and 0.1° in rotational direction was observed. The uncertainty results from a number of components in the imaging and registration process for the gray value algorithm is shown in Table VI. The uncertainties resulting from individual components in the image guidance process were less than 0.1 mm and 0.05° in all translational and rotational directions (Table VI).

Figure 3 shows the mean translational and rotational errors in all six directions for different image reconstruction and registration combinations available in XVI. The gray value and bone registration methods had mean error and standard deviation values ranging from −0.5($\sigma = 0.1$) to 0.3($\sigma = 0.1$) mm and −0.3($\sigma = 0.1$)° to 0.1($\sigma = 0.1$)° in translational and rotational directions.

TABLE IV. Expanded uncertainties in phantom rotational offsets measured when three different users set the phantom to preset rotational offsets.

Rotational axis	Expanded uncertainty with 95% confidence level
RX	0.06°
RY	0.06°
RZ	0.03°

TABLE V. Positional error values from XVI after verifying the phantom position on the treatment couch.

Translational errors (mm)			Rotational errors (deg)		
TX	TY	TZ	RX	RY	RZ
0.1	0.2	−0.2	0	0	−0.1

The mean error in the seed registration method showed sensitivity to image resolution. For the images with low resolution, the positional errors in translational and rotational directions ranged from $0.1(\sigma = 0.7)$ to $0.7(\sigma = 0.5)$ mm and $0.9(\sigma = 1.2)^\circ$ to $1.5(\sigma = 1.0)^\circ$, respectively. These errors reduced from $-0.1(\sigma = 0.3)$ to $0.3(\sigma = 0.3)$ mm and $-0.1(\sigma = 0.2)^\circ$ to $0.8(\sigma = 0.7)^\circ$ for images with medium resolution. For images reconstructed using the high resolution reconstruction algorithm, this error further reduced from $-0.2(\sigma = 0.1)$ to $0.4(\sigma = 0.1)$ mm and $-0.2(\sigma = 0.5)^\circ$ to $0.3(\sigma = 0.1)^\circ$.

III.C. Accuracy of positional offsets calculated by XVI

Figure 4(a) shows the reference and verification image datasets in axial, coronal, and sagittal planes before registration for one of the simulated positional offset studies (Set8 in Table III). Figure 4(b) shows the coregistered image datasets using gray value registration and XVI calculated positional offset values for the same study. Figure 5 shows the mean difference and standard deviation between the set and XVI predicted positional errors in each translational and rotational direction for the three different reconstructed resolutions. The calculated mean difference in each registration method is also shown in the same figure.

The gray value registration showed good agreement between the set and calculated positional offsets at all image resolutions. A maximum mean difference and standard deviation of $-0.2(\sigma = 0.4)$ mm in translational and $-0.1(0.1)^\circ$ in rotational directions was observed with gray value registration (Fig. 6). The bone registration with low resolution images showed a maximum difference of $-0.3(\sigma = 0.6)$ mm and $-0.6(\sigma = 1.0)^\circ$ in translational and rotational directions. In medium resolution images, a maximum mean difference of $-0.2(\sigma = 0.5)$ mm and $-0.4(\sigma = 0.4)^\circ$ was observed in translational and rotational directions. In high resolution images, this difference was reduced to $-0.2(\sigma = 0.4)$ mm and $-0.2(\sigma = 0.2)^\circ$ (Fig. 5). In the seed registration method, low resolution images showed large differences in calculated offsets; a maximum mean difference of $-0.4(\sigma = 0.9)$ mm and $-1.4(\sigma = 1.7)^\circ$ were observed in translational and rotational directions. This difference was reduced to $-0.2(\sigma = 0.3)$ mm and $-0.5(\sigma = 0.6)^\circ$ in medium resolution images. In high resolution images, this difference further reduced to $-0.1(\sigma = 0.2)$ mm and $-0.1(\sigma = 0.7)^\circ$.

TABLE VI. Uncertainties resulting from different components in the XVI imaging and registration process.

	TX	TY	TZ	RX	RY	RZ
Component studied	(mm)			(deg)		
Imaging and registration	0.00	0.00	0.00	0.02	0.00	0.00
KV source arm	0.02	0.00	0.02	0.02	0.00	0.02
KV detector arm	0.03	0.02	0.03	0.02	0.00	0.02
Different protocols	0.03	0.07	0.07	0.04	0.00	0.02

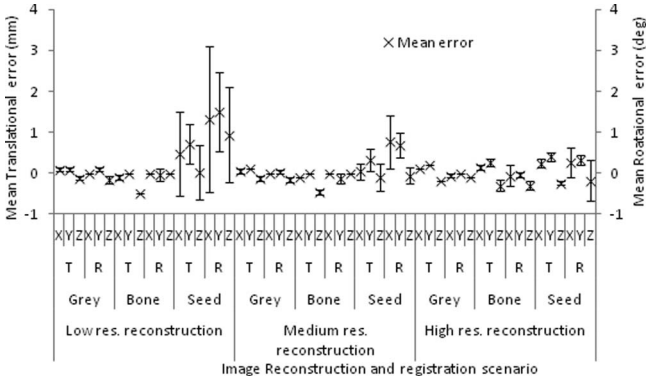

FIG. 3. Mean errors (with 1σ) in translational and rotational directions when the imaging and registration is performed under various possible combinations using XVI system.

III.D. Residual errors in overall image guidance and correction process

Figure 6 shows the mean residual errors and standard deviation in all six directions after the positional corrections were performed with the HexaPOD for verification for the offsets shown in Table III. The residual errors were within

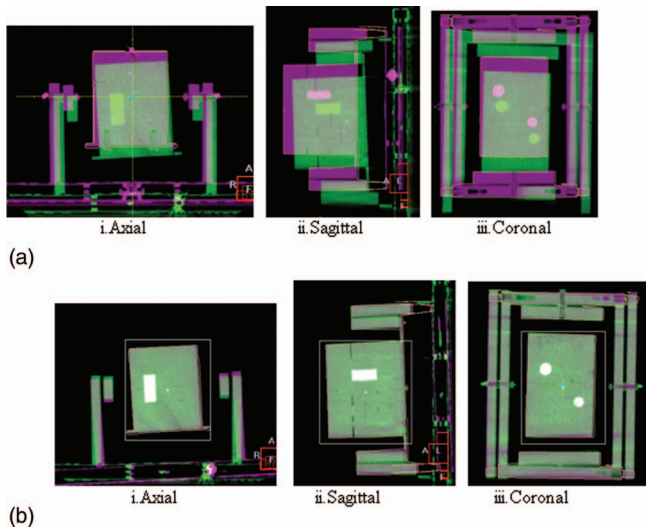

FIG. 4. (a) Reference and verification images of the phantom in (i) axial, (ii) sagittal, and (iii) coronal planes for one of the positional offsets (Set9) listed in Table III. (b) Coregistered reference and verification images of the phantom in (i) axial, (ii) sagittal, (iii) coronal planes for the same study. Verification images are reconstructed using high resolution reconstruction algorithm and registered with reference image using gray value registration method.

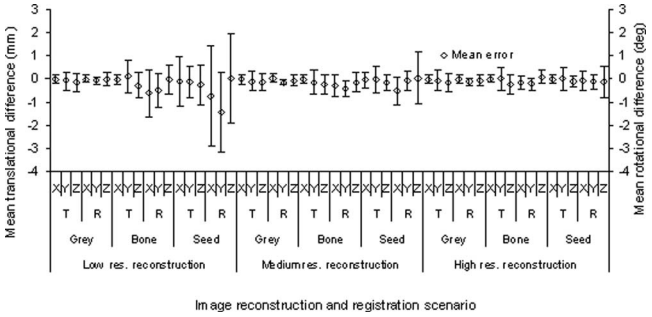

FIG. 5. Mean difference (with 1σ) between set and XVI calculated positional error values in all six directions for different image reconstruction and image registration combination for all offsets listed in Table III.

± 0.3 mm and $\pm 0.3^\circ$ in translational and rotational directions. Translational Y and rotational Z axes showed maximum mean residual errors of $0.1(\sigma = 0.2)$ mm and $-0.0(\sigma = 0.1)^\circ$, respectively.

IV. DISCUSSION

Many studies have shown that IGRT has the potential to reduce inter- and intrafractional uncertainties in patient positioning in the treatment room, thereby, providing the possibility to reduce the treatment margins with consideration of other relevant clinical factors.[17,18,23] However, image guidance systems have inherent limitations which result in residual errors in patient positional corrections. The residual errors that result from the image guidance process should be considered in margin reduction schemes. The phantom developed in this study enables verification of various rigid body registration methods available in commercial IGRT systems and to our knowledge is the first of its kind. The phantom enables the introduction of known positional offsets in all six directions simultaneously in conjunction with offsets via PSS. This enables the verification of positional errors calculated by registration algorithms and also verification of accuracy of the corrections performed via 6D-couch systems such as HexaPOD. Translational offsets can be set using the room lasers while rotational offsets can be introduced using the rotatable platform with a precision of $0.04(\sigma = 0.12)^\circ$, $0.02(\sigma = 0.13)^\circ$, and $-0.03(\sigma = 0.06)^\circ$ in X, Y, and Z directions. The higher precision in the Z direction (Fig. 2 and Table IV) is the result

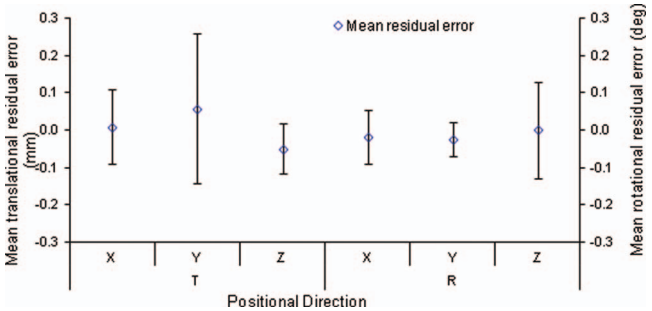

FIG. 6. Mean residual errors (with 1σ) in translational and rotational directions for corrections performed through HexaPOD couch for the offsets shown in Table III.

of the larger radius of the base of the rotatable platform which results in a larger linear distance between the graduations of scale. The positional accuracy and precision of the phantom is higher than the positional accuracy of the robotic couch reported in the literature[14,15] and this justifies the use of this phantom to test these systems.

One of the limitations in the current design of this phantom is that in addition to the rotational offsets, translational offsets also will be introduced if the treatment isocenter is placed other than at the phantom center in the reference image dataset. However, under these conditions the additional translational motion introduced can be easily calculated using simple Euclidean geometry relationships of the translational position of the new isocenter with respect to phantom center.

The uncertainty study performed in this investigation presented the precision of the XVI system for different image reconstruction and registration scenarios under controlled conditions. The gray value registration demonstrated small errors (in translation and rotational directions) in all image resolutions (Fig. 3). The error increased slightly (in translation and rotational directions) for the bone registration method in comparison with the gray value registration (Fig. 3). The seed registration method showed a strong sensitivity to image resolution with reduced errors as the image resolution increases (Fig. 3). As mentioned earlier, both the bone and seed registration methods implemented in XVI use chamfer algorithms, but the seed registration method matches small high density features present in the image data. The chamfer algorithm performs registration based on the edge information of two image datasets. The CBCT images reconstructed with low resolution result in large uncertainties in the seed registration method (Fig. 3) as the seed cross-sectional dimension is smaller than the image voxel size. This results in inaccurate edges of seeds in the verification image set and may lead to high uncertainties in use of the seed registration algorithm. The medium resolution images showed relatively less uncertainties in translational errors but the rotational errors were still high ranging from $-0.4(\sigma = 0.7)^\circ$ to $0.8(\sigma = 0.5)^\circ$. The high resolution images showed less uncertainty in the seed registration process suggesting the need for high resolution images while performing seed registration methods when rotational corrections are considered for clinical patient positions.

The positional offsets predicted by XVI showed similar trends for all registration algorithms (Fig. 5). This difference gradually reduced as the image resolution was increased. When large translational offsets were applied, the automatic registration often failed due to trapping of "local minima" in the defined region of interest in all registration methods. In such situations, initial verification images were aligned "roughly" with the reference set using manual registration methods and then the appropriate registration method under investigation was employed.

The main practical limitation of using high resolution reconstruction algorithm in daily CBCT image protocol is the longer reconstruction time. The XVI system uses an inline image reconstruction method during the image acquisition. In our clinical system when the low and medium resolution reconstruction algorithm was used in the imaging protocol, the

reconstructed image appeared for further study immediately after image acquisition. When high resolution reconstruction was used, it took an additional 76 s after image acquisition for the standard head and neck protocol used in this study. This time may be even greater for other imaging protocols with larger numbers of frames used for image acquisition. Clinically, this time difference for the higher resolution images may result in a negative impact on patient positioning accuracy as the time gap between the verification images and the initiation of treatment increases. The employment of greater computing power would solve this problem and would be well justified in a clinical setting.

Results from this study agree with previous studies. Lu *et al.*[24] evaluated the performance of the XVI image registration accuracy, using an anthropomorphic phantom, as a function of imaging dose. They achieved the positional offsets in translational and rotational directions by rotating and offsetting the reference image dataset and studied the accuracy of the gray value and bone registration methods. Lu *et al.*[24] found a maximum positional error in translational and rotational directions of 0.7 mm and 0.3°, respectively. Meyer *et al.*[15] completed a similar study using an anthropomorphic head and neck phantom with the positional offsets in their study performed through the movement of HexaPOD couch top. In their study, Meyer *et al.*[15] concluded that the gray value registration was more accurate than the bone registration and they also reported that the mean positioning accuracy of the XVI system in combination with Hexapod was under 0.3 mm and 0.3° in translational and rotational directions. Our study also showed similar conclusions for the gray value registrations. In addition, our study investigated the performance of the seed registration method and the sensitivity of different image registration methods to CBCT image resolution. One of the limitations in the present study is that we tested the performance of the seed registration method using one type of prostate seed. In practice, there are several varieties and sizes of prostate seeds in use. However, the seeds simulated in our phantom are the smallest of all commercially available seeds and thus represent the worst case scenario in a clinical situation.

Further, the phantom introduced in this study offers the possibility to introduce positional errors in all six directions simultaneously without the help of HexaPOD couch movements. Thus, it enables the user to perform an independent check of the accuracy of the XVI software and HexaPOD movements. The phantom is also useful to perform end-to-end testing of IGRT systems by introducing positional offsets in all six directions as well as providing an efficient option for performing routine quality assurance tests of image registration accuracy and HexaPOD table corrections.

The phantom presented in this study represents the best case scenario to test the overall performance of XVI and HexaPOD performance under controlled conditions. The accuracy of XVI and HexaPOD systems determined using the phantom represents the inherent accuracy of the system under controlled conditions. In reality, patient images are more complex with possible deformation of anatomic structures and out of plane rotations in the ROI of image registration during the course of treatment. Hence, the clinical decision to reduce setup margins should not be undertaken based on the performance of the system under controlled conditions rather margin reduction decision should be evaluated on a site-by-site basis together with consideration of system performance.

In the present study, the phantom was positioned close to the center of the FOV to assess the registration accuracy of XVI. Due to the relatively small size of the phantom, the image artifacts that might result from the half-field scanning mode in CBCT imaging and its impact on registration accuracy may not be captured. One of the purposes of the presented phantom is to provide an efficient tool to test the combined performance of the XVI and HexaPOD systems in routine clinical QA program. Due to this reason the size of the phantom was limited for easy use in routine practice. However, image registration accuracy with half-field scanning can be still tested using this phantom by positioning the phantom away from center of FOV.

V. CONCLUSION

A phantom developed as part of this study, capable of introducing known translational and rotational positional offsets was shown to be repositionable to within 0.06° in X and Y and 0.03° in Z directions, respectively. The phantom was used to demonstrate the accuracy of the XVI gray value registration method was independent of CBCT image resolution. The XVI seed registration method showed strong sensitivity to the image resolution with uncertainty converging to a minimum value as the image resolution increased. The overall residual error in the image guidance process of XVI in combination with the HexaPOD couch was less than 0.3 mm and 0.3° in translational and rotational directions when using the gray value registration with high resolution CBCT images. However, residual error, especially in rotational directions, may increase when the seed registration algorithm is used.

ACKNOWLEDGMENTS

The authors wish to acknowledge Standard Imaging Inc. USA for partial financial support of this project.

[a]Author to whom correspondence should be addressed. Electronic mail: Sankar.Arumugam@sswahs.nsw.gov.au; Telephone: +61 (0)2 87389413; Fax +61 (0)2 87389460.

[1]L. A. Dawson and D. A. Jaffray, "Advances in image-guided radiation therapy," J. Clin. Oncol. **25**(8), 938–946 (2007).
[2]J. J. W. Lagendijk, B. W. Raaymakers, A. J. E. Raaijmakers, J. Overweg, K. J. Brown, E. M. Kerkhof, R. W. van der Put, B. Hårdemark, M. van Vulpen, and U. A. van der Heide, "MRI/linac integration," Radiother. Oncol. **86**(1), 25–29 (2008).
[3]K. Langen, J. Pouliot, C. Anezinos, M. Aubin, A. Gottschalk, I. Hsu, D. Lowther, Y. Liu, K. Shinohara, and L. Verhey, "Evaluation of ultrasound-based prostate localization for image-guided radiotherapy," Int. J. Radiat. Oncol., Biol., Phys. **57**(3), 635–644 (2003).
[4]C. M. C. Ma and K. Paskalev, "In-room CT techniques for image-guided radiation therapy," Med. Dosim. **31**(1), 30–39 (2006).
[5]T. R. Mackie, J. Kapatoes, K. Ruchala, W. Lu, C. Wu, G. Olivera, L. Forrest, W. Tome, J. Welsh, and R. Jeraj, "Image guidance for precise con-

formal radiotherapy," Int. J. Radiat. Oncol., Biol., Phys. **56** (1), 89–105 (2003).
[6]R. Kamath, T. C. Ryken, S. L. Meeks, E. C. Pennington, J. Ritchie, and J. M. Buatti, "Initial clinical experience with frameless radiosurgery for patients with intracranial metastases," Int. J. Radiat. Oncol., Biol., Phys. **61**(5), 1467–1472 (2005).
[7]M. W. K. Kan, L. H. T. Leung, W. Wong, and N. Lam, "Radiation dose from cone beam computed tomography for image-guided radiation therapy," Int. J. Radiat. Oncol., Biol., Phys. **70**(1), 272–279 (2008).
[8]J. P. Bissonnette, P. A. Balter, L. Dong, K. M. Langen, D. M. Lovelock, M. Miften, D. J. Moseley, J. Pouliot, J. J. Sonke, and S. Yoo, "Quality assurance for image-guided radiation therapy utilizing CT-based technologies: A report of the AAPM TG-179," Med. Phys. **39**(4), 1946–1963 (2012).
[9]E. Osei, R. Jiang, R. Barnett, K. Fleming, and D. Panjwani, "Evaluation of daily online set-up errors and organ displacement uncertainty during conformal radiation treatment of the prostate," Br. J. Radiol. **82**(973), 49–61 (2009).
[10]A. R. Yeung, J. G. Li, W. Shi, H. E. Newlin, A. Chvetsov, C. Liu, J. R. Palta, and K. Olivier, "Tumor localization using cone-beam CT reduces setup margins in conventionally fractionated radiotherapy for lung tumors," Int. J. Radiat. Oncol., Biol., Phys. **74**(4), 1100–1107 (2009).
[11]R. B. Den, A. Doemer, G. Kubicek, G. Bednarz, J. M. Galvin, W. M. Keane, Y. Xiao, and M. Machtay, "Daily image guidance with cone-beam computed tomography for head-and-neck cancer intensity-modulated radiotherapy: A prospective study," Int. J. Radiat. Oncol., Biol., Phys. **76**(5), 1353–1359 (2010).
[12]M. Guckenberger, J. Meyer, D. Vordermark, K. Baier, J. Wilbert, and M. Flentje, "Magnitude and clinical relevance of translational and rotational patient setup errors: A cone-beam CT study," Int. J. Radiat. Oncol., Biol., Phys. **65**(3), 934–942 (2006).
[13]D. C. Hornick, D. W. Litzenberg, K. L. Lam, J. M. Balter, J. Hetrick, and R. K. Ten Haken, "A tilt and roll device for automated correction of rotational setup errors," Med. Phys. **25**, 1739–1740 (1998).
[14]M. Guckenberger, J. Meyer, J. Wilbert, K. Baier, O. Sauer, and M. Flentje, "Precision of image-guided radiotherapy (IGRT) in six degrees of freedom and limitations in clinical practice," Strahlenther. Onkol. **183**(6), 307–313 (2007).
[15]J. Meyer, J. Wilbert, K. Baier, M. Guckenberger, A. Richter, O. Sauer, and M. Flentje, "Positioning accuracy of cone-beam computed tomography in combination with a HexaPOD robot treatment table," Int. J. Radiat. Oncol., Biol., Phys. **67**(4), 1220–1228 (2007).
[16]*XVI R4.5 Instructions for Use* (Elekta AB, Stockholm, Sweden, 2009).
[17]M. Enmark, S. Korreman, and H. Nyström, "IGRT of prostate cancer; is the margin reduction gained from daily IG time-dependent?" Acta Oncol. **45**(7), 907–914 (2006).
[18]I. S. Grills, G. Hugo, L. L. Kestin, A. P. Galerani, K. K. Chao, J. Wloch, and D. Yan, "Image-guided radiotherapy via daily online cone-beam CT substantially reduces margin requirements for stereotactic lung radiotherapy," Int. J. Radiat. Oncol., Biol., Phys. **70**(4), 1045–1056 (2008).
[19]A. Roche, G. Malandain, X. Pennec, and N. Ayache, "The correlation ratio as a new similarity measure for multimodal image registration," in *Proceedings of the Medical Image Computing and Computer-Assisted Intervention—MICCAI'98* (Springer Verlag, Cambridge MA, 1998), pp. 1115–1124.
[20]G. Brogefors, "Hierarchical chamfer matching: A parametric edge matching algorithm," IEEE Trans. Pattern Anal. Mach. Intell. **10**, 849–865 (1988).
[21]D. Létourneau, A. A. Martinez, D. Lockman, D. Yan, C. Vargas, G. Ivaldi, and J. Wong, "Assessment of residual error for online cone-beam CT-guided treatment of prostate cancer patients," Int. J. Radiat. Oncol., Biol., Phys. **62**(4), 1239–1246 (2005).
[22]D. Létourneau, J. W. Wong, M. Oldham, M. Gulam, L. Watt, D. A. Jaffray, J. H. Siewerdsen, and A. A. Martinez, "Cone-beam-CT guided radiation therapy: Technical implementation," Radiother. Oncol. **75**(3), 279–286 (2005).
[23]O. Nairz, F. Merz, H. Deutschmann, P. Kopp, H. Schöller, F. Zehentmayr, K. Wurstbauer, G. Kametriser, and F. Sedlmayer, "A strategy for the use of image-guided radiotherapy (IGRT) on linear accelerators and its impact on treatment margins for prostate cancer patients," Strahlenther. Onkol. **184**(12), 663–667 (2008).
[24]B. Lu, H. Lu, and J. Palta, "A comprehensive study on decreasing the kilovoltage cone-beam CT dose by reducing the projection number," J. Appl. Clin. Med. Phys. **11**(3), 231–249 (2010).